

Parameter-Based Design and Analysis of Wind Turbine Airfoils with Conformal Slot Co-Flow Jet

C. Y. Ma and H. Y. Xu[†]

National Key Laboratory of Science and Technology on Aerodynamic Design and Research, Northwestern Polytechnical University, Xi'an, 710072, China

[†]*Corresponding Author Email: xueyong@nwpu.edu.cn*

(Received May 23, 2022; accepted September 27, 2022)

ABSTRACT

A co-flow jet (CFJ), an active flow control method combining blowing and suction control, can effectively suppress the stall of airfoils. However, the streamwise jet channel along the upper surface of a conventional CFJ airfoil reduces the thickness and camber of the baseline, degrading the aerodynamic performance when the jet is inactive. The conformal slot CFJ airfoil was proposed to address this problem, but the design method is still absent. This paper proposed a general design method based on parameters including the slot angle, transition shape and distance of the injection and suction slot. The mechanism of the best parameter was analyzed. The designed conformal slot CFJ airfoil was checked under different jet intensities, and the turbine power curve was predicted when substituting CFJ airfoils for the baseline. Compared with the conventional CFJ airfoil, the designed conformal slot CFJ airfoil has three advantages: eliminating the performance loss when the jet is off, saving jet energy when suppressing the flow separation, and improving the power generation of wind turbines at low wind speeds.

Keywords: Co-flow jet; Wind turbine airfoil; Conformal slot; Blowing; Suction; Flow control.

NOMENCLATURE

A_i	area of injection slot	P_c	jet power consumption coefficient
A_s	area of suction slot	P_e	output power coefficient of a wind turbine blade element
c	chord	r	blade element radius
c_p	specific heat at constant pressure	T_s^*	total temperature of suction
C_μ	jet momentum coefficient	V_∞	velocity of incoming flow
C_l	lift coefficient	V_i	averaged velocity of injection
C_d	drag coefficient	V_s	averaged velocity of suction
C_{dc}	corrected drag coefficient including power consumption and drag coefficient	W	resultant velocity of blade element
F_l	total lift of CFJ airfoils	α	angle of attack
F_d	total drag of CFJ airfoils	γ	ratio of specific heat at constant pressure and constant volume
F_{lr}	reaction force of injection and suction in lift direction	η	pump efficiency
F_{dr}	reaction force of injection and suction in drag direction	θ	designed pitch angle of blade elements
F_{ls}	surface force of CFJ airfoils in lift direction	$\theta_{i,mv}$	angle of momentum of injection slot
F_{ds}	surface force of CFJ airfoils in drag direction	$\theta_{s,mv}$	angle of momentum of suction slot
\dot{m}	mass flow rate of jet	$\theta_{i,PA}$	angle of pressure force of injection slot
P_i	pressure on injection slot	$\theta_{s,PA}$	angle of pressure force of suction slot
P_s	pressure on suction slot	ρ_∞	density of incoming flow
P_i^*	total pressure on injection slot	Φ	designed inflow angle of blade elements
P_s^*	total pressure on suction slot	ω	rotor speed of wind turbine

1. INTRODUCTION

Wind energy plays a vital role in various renewable energies (International Energy Agency 2021). An increase in the output power of an individual wind turbine directly contributes to the global emission target. However, the incoming airflow to wind turbines is usually unstable due to atmospheric boundary layer shear, atmospheric turbulence and yaw in the wind direction, making wind turbines often subject to dynamic stalls (Choudhry *et al.* 2013; Mamouri *et al.* 2019; Zhu *et al.* 2021). In addition, wind turbines cannot generate power efficiently when the wind speed is lower (Singh and Ahmed 2013; Rafiuddin *et al.* 2018; Fan and Zhu 2019). Therefore, to increase the output power of an individual wind turbine, it is necessary to improve the aerodynamic performance before and after the stall.

The flow control technique is a feasible method to increase the output power of wind turbines (Aramendia *et al.* 2017; Aubrun *et al.* 2017). This technique can be divided into active flow control (AFC) and passive flow control (PFC) (Gad-el-Hak 2000). Van Dam *et al.* (2008), and Johnson *et al.* (2010) proposed a labeling scheme to classify 15 AFC techniques showing potential for wind turbine control. According to the classification, the blowing/suction method can shift the lift curve before the stall and suppress flow separation after the stall. Therefore, studying its flow control effect in wind turbines is valuable because of its unique characteristics.

The difficulty of applying blowing/suction technology to wind turbines lies in the air sources, power consumption and installation. However, Car *et al.* (2004) and Zha *et al.* (2004) proposed the co-flow jet (CFJ) concept, which combines blowing and suction technologies on airfoils or wings by translating a section of suction surface downward to construct a streamwise jet channel. This concept solves the problems of air source, energy consumption and installation to a certain extent. The blowing jet near the leading edge can be recycled through the suction slot near the trailing edge, reducing jet power consumption compared with the pure blowing or suction due to the relatively higher total pressure of the recycled jet flow. The air source can be provided by micropumps installed inside the wing or blade. In the field of aviation, the CFJ concept has been studied extensively. It has been revealed that this method can contribute to ultrahigh lift and ultrahigh aerodynamic efficiency (Liu *et al.* 2016; Dhakal *et al.* 2017; Yang and Zha 2017, 2018; Wang and Zha 2019). These characteristics led to a significant amount of research on CFJs on aircraft components. Several conceptual aircraft using CFJ technology have been proposed including the CFJ-EA (Yang and Zha 2018), CFJ-HERA (Yang and Zha 2019) and CFJ-VTOL (Boling *et al.*, 2021). For CFJ research on helicopters, Lefebvre and Zha (2013, 2014) researched the dynamic stall suppression of the rotor airfoil through CFJ at Mach 0.3 and 0.4. Liu *et al.* (2020, 2022a, 2022b) further investigated the dynamic stall suppression of a rotor

airfoil at Mach 0.14, 0.15 and 0.7 and a 3D blade at rotor-tip Mach 0.6 using the CFJ method. Recently, some novel CFJ studies were proposed. Wu *et al.* (2020) investigated the performance enhancement of flapping airfoils by CFJ. Byrd *et al.* (2021) designed a high-endurance rotating-wing mars exploration spacecraft using CFJ technology. Following these studies of CFJs in aviation and aerospace, Xu *et al.* (2015, 2016) studied the effect of CFJs on a wind turbine airfoil (S809) by numerical simulation. The steady cases showed that CFJ has significant positive effects on the increasing lift, stall margin and drag reduction (Xu *et al.* 2015). In the pitching case, the dynamic stall was greatly suppressed, and the extreme aerodynamic loads were significantly alleviated (Xu *et al.* 2016). An energy consumption analysis showed that the CFJ is an economical AFC method for delaying or controlling stalls (Xu *et al.* 2015; 2016). Xu *et al.* (2020) further optimized the injection and suction parameters of the CFJ-S809 airfoil. The optimum configuration can increase the max lift coefficient by 42.3% with a similar or higher lift-to-drag ratio even when considering the jet power consumption. Zhang *et al.* (2021a) proposed an adaptive jet momentum coefficient strategy using the CFJ-S809 airfoil and checked it using the PHASE VI wind turbine blade by the blade element - moment (BEM) theory method. Xu *et al.* (2021) further investigated the output power improvement of wind turbine blades with CFJs by the Reynolds-averaged Navier-Stokes (RANS) method and proved that the CFJ is particularly useful for wind turbines.

Compared with the aviation field, the application of CFJs in wind turbines is more convenient. On the one hand, the lower wind speed of wind turbines reduces the requirements for the jet speed. On the other hand, there is enough space inside the wind turbine blade to install the pump and motive power system, such as batteries and wiring, especially in the inboard part where thick airfoils were used. Because there are peaks and valleys in electricity demand during the day and night, the motive power system of the CFJ can be charged with the off-peak power, which can be from the wind turbine itself or the power grid. The CFJ is turned on when flow separation occurs. However, the conventional CFJ airfoil has a lower lift coefficient than the baseline when the jet is inactive, as the streamwise jet channel reduces the thickness and camber of the baseline. It can be inferred that a wind turbine with CFJ airfoil produces more output power if the CFJ technology eliminates the jet channel, which benefits from the jet effect and the unreduced thickness and camber of the baseline. Moreover, the baseline performance is maintained if the jet and suction slot are blocked or the jet system fails.

To eliminate the adverse effects of the jet channel, Chng *et al.* (2008) and Zhang *et al.* (2011) proposed a conformal slot CFJ airfoil in which the majority of the airfoil suction surface remains the same as the baseline but the local geometry close to the injection and suction slot is shaped to guide the flow tangential to the local airfoil surface. Genç *et al.* (2011) investigated two kinds of CFJ (blowing before suction and suction before blowing) without

modifying the baseline, but the boundary conditions of the injection and suction slot are virtual, ignoring the transition from the slot to the upper surface. Liu *et al.* (2016) studied the effect of the suction slot angles of a CFJ airfoil with 0.1%*c* airfoil suction surface translations (SSTs), similar to the conformal slot CFJ concept, but they only investigated two suction slot angles (12° and 78°) and did not consider the effect of the local shape between the slot and the airfoil surface. Xu *et al.* (2019) proposed three methods to avoid the negative effect of the jet channel when the jet is inactive. One of these methods uses a small moving surface to cover the injection and suction slot. This is also based on a conformal slot design, but the detailed design method of the conformal slot was not proposed. Zhang *et al.* (2021) investigated a pulsed CFJ based on a designed conformal slot, but they also did not give the design method and did not compare it with a conventional CFJ airfoil when the jet is active. Liu *et al.* (2022b) find that the sloping slot, a kind of conformal slot, is more effective in suppressing the shock-induced dynamic stall and the dynamic stall at low speed and high angles of attack. The works mentioned above are all concerned with conformal slot design, but most conformal slot designs depend on experience, and a detailed mechanism analysis of the conformal slot CFJ is absent. Therefore, it is necessary to propose a general design method for the conformal slot CFJ and explore the aerodynamic mechanism.

This paper proposed a general design method based on slot parameters for the conformal slot CFJ. Although much work has been done on the CFJ parameters (Zha *et al.* 2006; Wang and Zha 2019; Zhi *et al.* 2021), most of these studies were not aimed at canceling the jet channel, so the transition shape and transition distance were not addressed. The parameters of the conformal slot CFJ are similar to those of the vortex generator (VG) jet if only considering the injection slot. However, the mechanism of the VG jet produces a pair of streamwise vortices, which is different from the CFJ, where the attached jet flow is needed. The proper transition shape from the slot to the airfoil surface is critical for CFJ, whereas the VG jet does not need to consider the transition, so the jet hole of the VG jet is inserted at a constant angle to the airfoil surface

(Johnston *et al.* 1990; Laval *et al.* 2010; Shun and Ahmed 2012; Prince *et al.* 2017). As the novelty for this paper, the transition shape from the slot to the airfoil surface was classified into three types, and the effect of these three transition shapes was investigated combined with the slot angle and transition distance. Moreover, to facilitate the calculation of the CFJ reaction force for different slot angles, general formulas for the CFJ reaction force were proposed. In addition, power consumption must be considered for the AFC method, so all parameters were evaluated under the same power consumption coefficient, which is different from previous studies and more intuitive when selecting the best parameters. The rest of this paper is organized as follows: Section 2 describes the geometry and aerodynamic parameters of the CFJ and the conformal slot CFJ airfoil design method. Section 3 presents the numerical method and validation results. Section 4 presents the design process and results based on the parameters. Section 5 discusses the performance under different jet intensities and evaluates the effect of the conformal slot CFJ on a wind turbine. Section 6 ends this paper with some conclusions.

2. DESIGN METHOD OF CONFORMAL SLOT CFJ AIRFOIL

The conventional and conformal slot CFJ airfoil model, the aerodynamic parameters used in the design process and the design procedure are introduced in this section.

2.1 CFJ Airfoil and Geometric Parameters

The S809 airfoil (Somers *et al.* 1997) was used as the baseline, as it was designed specifically for the stall regular wind turbine. The stall characteristic was prominent, so it is suitable for separation flow control research. Figure 1 shows the difference between the conformal slot CFJ airfoil (colored lines) and the conventional CFJ airfoil. The injection and suction slots were set at 6.0%*c* and 80.0%*c* from the leading edge with heights of 0.65%*c* and 1.38%*c*, respectively. The specific design parameters of the conventional CFJ airfoil can be found in Xu *et al.* (2015).

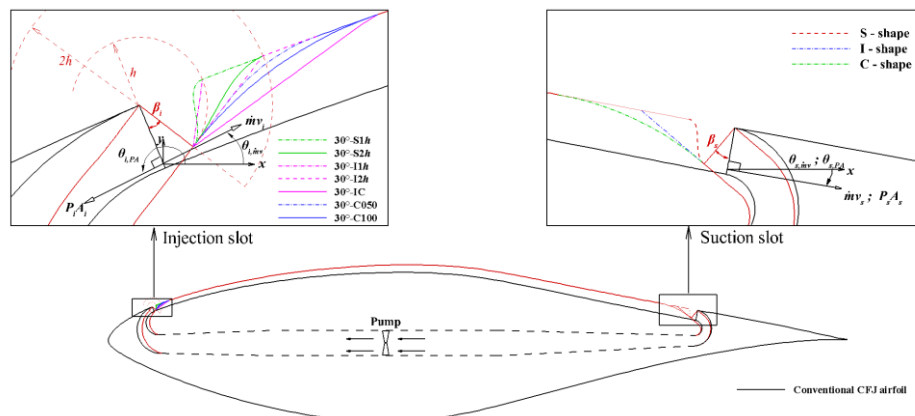


Fig. 1. Geometry of conventional and conformal slot CFJ airfoil.

Figure 1 shows that the streamwise jet channel of the conventional model on the upper surface between the injection and suction slot reduces the thickness and camber of the baseline. The conformal slot CFJ airfoil has the same geometry as the baseline except for the local positions near the injection and suction slot. Three parameters of the conformal slot determine the final shape near the injection and suction slot. The first parameter is the slot angle, β_i and β_s , which represent the injection angle and suction angle, respectively. This is the angle between the slot surface of the conformal and conventional model. The second parameter is the transition form. Taking the suction slot in Fig. 1 as an example, all possible transition forms can be classified into S-shape, I-shape and C-shape. The third parameter is the transition distance, parameterized by the slot height (h) and determined by the slot angle and transition form.

Taking the injection slot with a 30° slot angle as an example, the seven transition shapes in Fig. 1 represent all possible parameterized transition types. The 30°-S1 h and 30°-I1 h represent typical transition shapes in which the transition distance equals the slot height. In these two cases, the jet direction and the injection slot surface were at an acute angle, which results in compression of the jet flow to a certain extent. The 30°-S2 h , 30°-I2 h , 30°-C050 and 30°-C100 represent four typical transition shapes in which the jet direction is normal to the injection slot surface. The transition distances of 30°-S2 h and 30°-I2 h were close to twice the height of the slot. The C-shape transition form was formed by a chamfering design based on the I-shape and is perpendicular to the slot surface. Many C-shapes can be formed according to the different starting positions of chamfering. In this paper, chamfering was carried out at the midpoint and starting point of the 30°-I2 h shape to form two C-shapes named 30°-C050 and 30°-C100. The 30°-IC is an I-shaped transition form with the same transition distance as 30°-C100, but the jet direction and the slot surface are at an obtuse angle, which might be easier for blowing.

2.2 Aerodynamic Parameters of CFJ Airfoil

For CFJ airfoils, the jet intensity is usually quantified by the jet momentum coefficient, which is defined as

$$C_\mu = \frac{\dot{m}V_j}{\frac{1}{2}\rho_\infty V_\infty^2 c} \quad (1)$$

When calculating the lift and drag of the CFJ airfoil, the reaction force of the injection and suction slot in the lift and drag direction should be considered. [Zha et al. \(2007\)](#) proposed a formula for the conventional CFJ airfoil, where the injection slot is backward and the suction slot is forward. This paper proposed improved formulas for the reaction force that apply to any direction or slot angle of the injection and suction slots. The formulas are as follows:

$$F_{lr} = -\dot{m}V_i \sin(\theta_{i,mv} - \alpha) + P_i A_i \sin(\theta_{i,PA} - \alpha) + \dot{m}V_s \sin(\theta_{s,mv} - \alpha) + P_s A_s \sin(\theta_{s,PA} - \alpha) \quad (2)$$

$$F_{dr} = -\dot{m}V_i \cos(\theta_{i,mv} - \alpha) + P_i A_i \cos(\theta_{i,PA} - \alpha) + \dot{m}V_s \cos(\theta_{s,mv} - \alpha) + P_s A_s \cos(\theta_{s,PA} - \alpha) \quad (3)$$

The sign conventions for $\theta_{i,mv}$, $\theta_{s,mv}$, $\theta_{i,PA}$ and $\theta_{s,PA}$ are positive when measured counterclockwise from the horizontal line to the direction of $\dot{m}V_i$, $\dot{m}V_s$, $P_i A_i$ and $P_s A_s$. A schematic diagram of the CFJ reaction force is shown in Fig. 1.

The total aerodynamic force coefficient for a CFJ airfoil is the sum of the reaction force on the injection and suction slot and the airfoil surface force, so the lift coefficient and drag coefficient are as follows:

$$C_l = \frac{F_l}{\frac{1}{2}\rho_\infty V_\infty^2 c} = \frac{F_{ls} + F_{lr}}{\frac{1}{2}\rho_\infty V_\infty^2 c} \quad (4)$$

$$C_d = \frac{F_d}{\frac{1}{2}\rho_\infty V_\infty^2 c} = \frac{F_{ds} + F_{dr}}{\frac{1}{2}\rho_\infty V_\infty^2 c} \quad (5)$$

The power for the jet system can be computed using the following equation:

$$P = \frac{\dot{m}c_p T_s^*}{\eta} \left[\left(\frac{P_i^*}{P_s^*} \right)^{\frac{\gamma-1}{\gamma}} - 1 \right] \quad (6)$$

where $\gamma=1.4$ and $\eta=80\%$. The power consumption can be converted to drag, and then the aerodynamic efficiency of the CFJ airfoil is evaluated by the corrected lift-to-drag ratio:

$$\frac{C_l}{C_{dc}} = \frac{C_l}{C_d + P_c} \quad (7)$$

where

$$P_c = \frac{P}{\frac{1}{2}\rho_\infty V_\infty^3 c} \quad (8)$$

2.3 Design Procedure

In the conformal slot design process, the power consumed by the jet system, also representing the jet intensity, was set to a constant value. Thus, only the lift coefficient and the corrected lift-to-drag ratio (also referred to as the aerodynamic efficiency) should be evaluated to choose the optimal parameter. The design process is shown in Fig. 2. First, only the injection slot parameters are considered, with the best transition form chosen by comparing the seven typical transition shapes in Fig. 1. at a given injection angle. Second, the best slot angle is chosen by comparing different slot angles based on the best transition form in the previous step. Finally, the suction slot parameters are compared using the same methods mentioned above to specify the best suction parameters.

The conformal slot CFJ airfoil in this paper was named using the following convention: CFJ809-I β iXi-S β sXs, where β_i and β_s were replaced by the injection and suction slot angle, and Xi and Xs were replaced by the transition shape and distance (if the distance were needed) of injection and suction slots, respectively. For example, CFJ809-I45C-S30S2 h

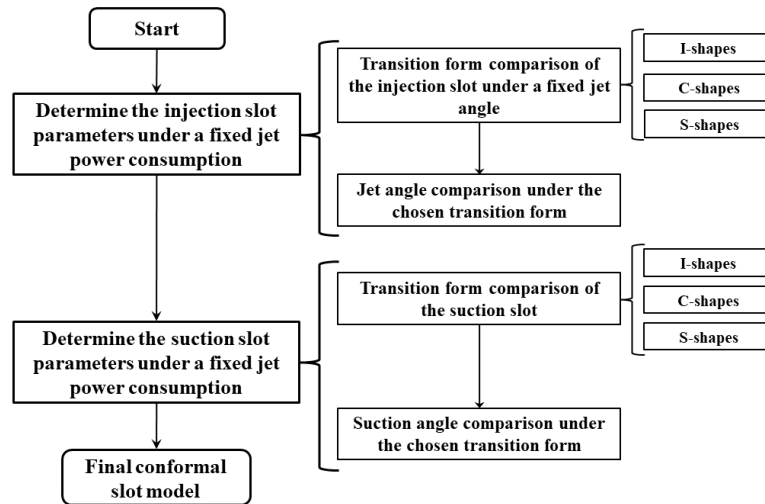


Fig. 2. Flowchart of conformal slot design procedure.

has a 45° jet angle and 30° suction angle, then the transition shape of the injection slot is C-shaped. The transition shape of the suction slot is S-shaped with a transition distance of $2h$.

3. COMPUTATIONAL MODEL AND VALIDATION

3.1 Numerical Method and Boundary Conditions

The simulation was performed numerically using the computational fluid dynamics software Fluent® by solving the RANS equations and the Spalart-Allmaras (S-A) turbulence model. The S-A turbulence model can better predict the boundary layer in the presence of adverse pressure gradients, so it is often used in the simulation of airfoil aerodynamics and other outer flow simulations. The coupled algorithm is employed for the pressure-velocity coupling. The second-order upwind was used in the spatial discretization. The computation domain, mesh and boundary condition are shown in Fig. 3. Two ducts twice the height of the slot height

were added to the injection and suction slots to ensure the velocity profile of the jet flow. The airfoil, injection and suction duct were set to no-slip wall boundary conditions. The jet inlet was set to the pressure inlet boundary condition. The jet outlet was set to the pressure outlet boundary condition. The injection and suction slots were set to interior boundary conditions to acquire the pressure and momentum on slots for calculating the jet reaction force. The pressure far-field boundary condition was used for the outer boundary of the computed zone, in which the distance is $50c$ from the location of the airfoil.

When the jet is active, the total pressure at the jet inlet boundary is adjusted by a user-defined function (UDF) to reach the predetermined power consumption coefficient. In addition, to ensure the zero-net-mass-flux of the CFJ system, the static pressure at the jet outlet boundary was adjusted by another UDF to inhale the same mass flow rate as the jet flow from the injection slot. When the jet is inactive, the jet inlet and the jet outlet are set to wall boundary conditions.

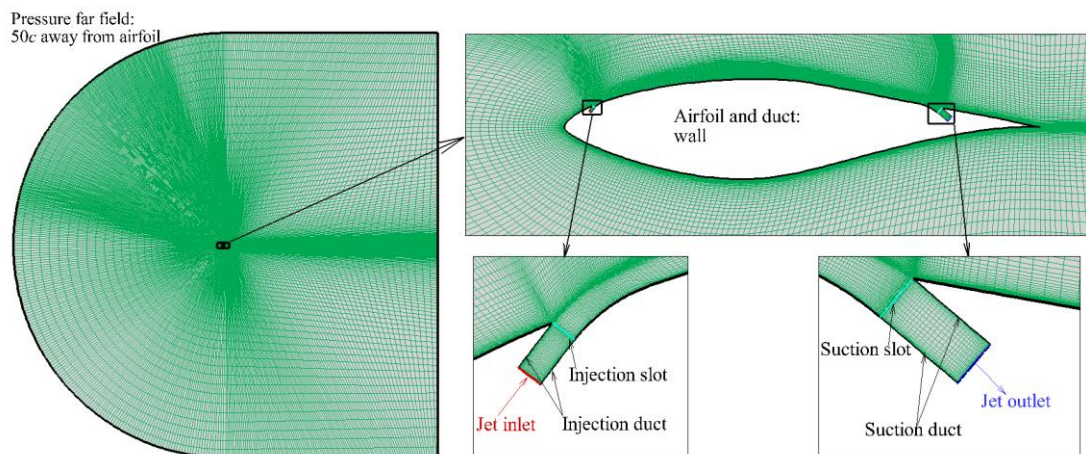


Fig. 3. Schematic of computation domain, mesh and boundary conditions.

3.2 Method Validation

The author's previous research involves the simulation of the CFJ809 airfoil (Xu *et al.* 2015; 2016) using an in-house CFD code. The force generated by the blowing and suction was calculated using the force formula for a conventional CFJ airfoil proposed by Zha *et al.* (2007). This paper uses Eq. (2)-(5) to calculate the lift and drag coefficient, including the reaction force of the blow and suction. The newly proposed force formulas and the numerical method used in this paper were validated by comparing the present simulation results with previous results (Xu *et al.* 2015). Figure 4 shows the validation results when the jet momentum is 0.06. The lift and drag coefficients of this paper are consistent with those in previous research. The minor difference may come from the setting of the CFD solver and numerical error, but certainly the numerical method and the proposed CFJ reaction force formulas in this paper are capable of the design and parameter research for the CFJ.

3.3 Grid Sensitivity Study for Conformal Slot CFJ Airfoil

Before the conformal slot design and parameter study, a grid sensitivity analysis of the conformal slot CFJ airfoil was performed. The model used for the grid sensitivity study is shown in Fig. 3. The injection and suction angles of the model were 30° , and the C-shape transition type was used. The Reynolds number was set to 2.0×10^6 , and the Mach number was 0.15. A total of 6 sets of grids were compared, and the number of grids was 29,456, 44,319, 90,504, 177,487, 349,017 and 682,950. The first layer spacing was $2 \times 10^{-5}c$, $1.5 \times 10^{-5}c$, $1.0 \times 10^{-5}c$, $0.7 \times 10^{-5}c$, $0.5 \times 10^{-5}c$ and $0.36 \times 10^{-5}c$. The growth rate of the wall grid was 1.05, the number of grid layers in the boundary layer was 30, and y^+ was less than 1. These grids were computed at 10° , 20° and 30° angles of attack, and the results are shown in Fig. 5. These three angles of attack correspond to the attached flow, medium separation flow and complete separation flow, respectively. It can be seen that the variation in the force coefficients after grid three is very small when the angles of attack are 10° and 20° . When the flow is completely separated, these six grids show similar results. Therefore, given the computational accuracy and cost, grid three was used for the design research.

4. DESIGN AND ANALYSIS OF CONFORMAL SLOT CFJ AIRFOIL

4.1. Design and Analysis of Conformal Injection Slot

This study of the injection slot parameters did not consider the suction slot. Therefore, it is assumed that the jet was drawn in from the free stream and pressurized to a predetermined jet intensity, and the geometry is the baseline (S809 airfoil) equipped with a pure-blowing jet, similar to the model in Fig. 3. without the suction slot. It is also possible to add a suction slot to the baseline and keep it active, but this situation is not considered here since the suction only provides a control enhancement effect but does not

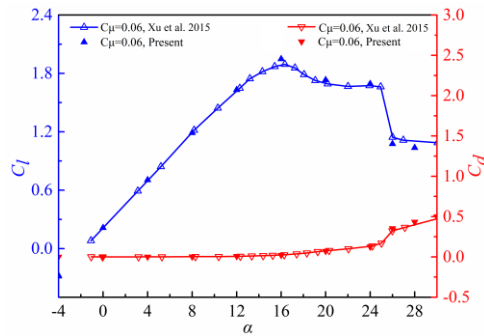


Fig. 4. Validation of newly proposed CFJ force formula and numerical method by comparison with previous simulation of Xu *et al.* (2015).

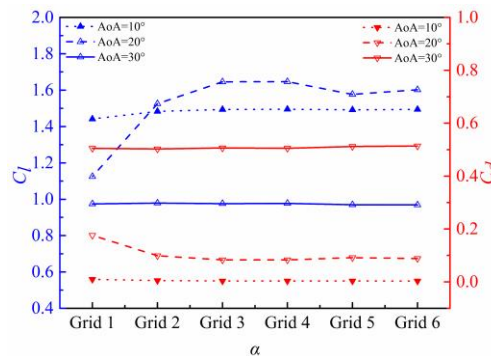


Fig. 5. Results of mesh sensitivity validation.

affect the comparison trend of the injection parameters. To facilitate comparison, the conventional CFJ airfoil (CFJ809) in this section only kept the injection slot open, and the suction slot was set to the wall boundary condition. The transition shapes were compared, and then five jet angles (0° , 15° , 30° , 45° and 60°) were compared based on the optimal transition shape.

Figure 6 shows the aerodynamic performance of seven transition shapes. As shown in Fig. 6(a), 30° -C100 possesses the best ability to improve the lift coefficient. Although the CFJ809 airfoil offers the highest lift coefficient, there is a noticeable lift loss in the linear zone compared to most conformal injection slot shapes. This is due to the reduction in airfoil thickness and camber caused by the streamwise jet channel. The performance deteriorates when the transition distance is the same as the injection slot height whether an S-shape (30° -S1h) or an I-shape (30° -I1h) is used. However, the performance of the S-shape is always better than that of the I-shape, particularly when the transition distance is specified as twice the height of the injection slot (30° -S2h and 30° -I2h). Figure 6(b) shows that the 30° -IC shape exhibits the best aerodynamic efficiency, followed by the 30° -C100 shape. Figure 6(c) shows that the 30° -IC exhibits the worst lift coefficient when the jet is inactive because of the most apparent change on the baseline, making the negative effect of the jet channel more pronounced than the others. Considering the aerodynamic performance when the jet is on and off, the C100 shape is considered the best among these transition shapes.

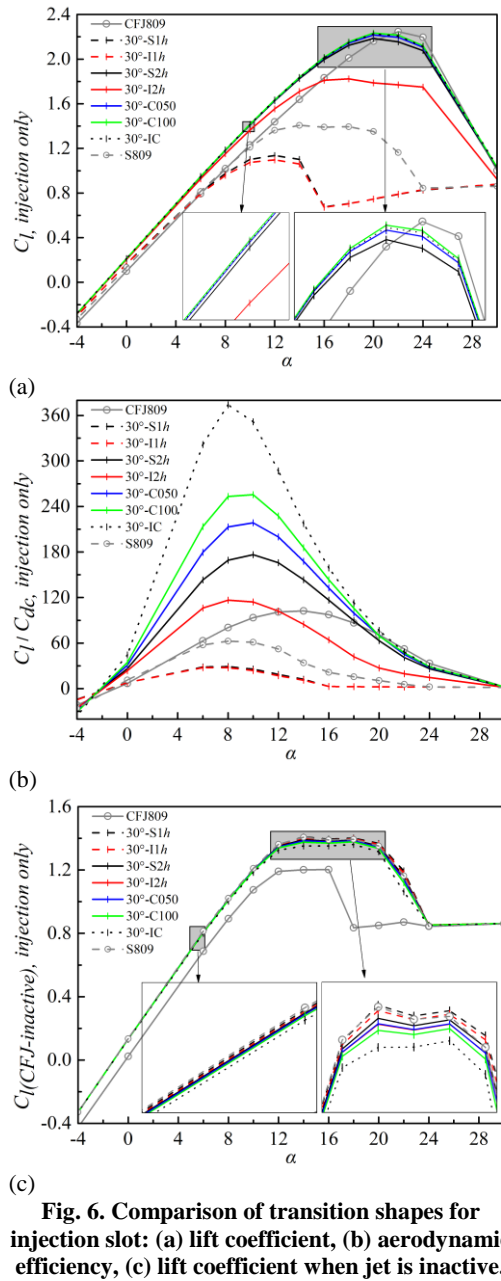
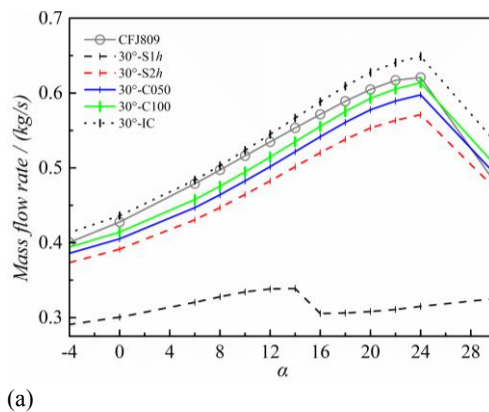


Fig. 6. Comparison of transition shapes for injection slot: (a) lift coefficient, (b) aerodynamic efficiency, (c) lift coefficient when jet is inactive.

The reason for Fig. 6(b) is that the 30°-IC shape has the largest actual jet angle under its slot angle. It is



easier for the jet flow to expel under the same pump power consumption. Therefore, the 30°-IC shape has the largest mass flow rate in the injection slot, as shown in Fig. 7(a), which means more jet thrust (the negative drag coefficient), as shown in Fig. 7(b), making the 30°-IC shape have the highest aerodynamic efficiency even though its lift coefficient is lower than the 30°-C100 shape. CFJ809 has the most significant jet thrust, as shown in Fig. 7(b), because its jet reaction force has more components in the thrust direction, which benefits from its 0° jet angle. However, the closed suction slot and the streamwise jet channel bring more drag, which offsets the thrust. Hence, the CFJ809 injection-only case has lower aerodynamic efficiencies.

The C-shape (we refer only to C100 from this point) was combined with different injection angles to evaluate its performance. However, as shown in Fig. 1, the C-shape has the longest transition distance when the jet direction is normal to the slot. To avoid a deterioration in aerodynamic performance due to the apparent change in the baseline because of the long transition distance when the jet is inactive, the C-shape is selected only when the injection angle is larger than 30°, and the S-shape combined with three transition distances of 2h, 3h and 4h are adopted when the injection angle is less than 30°. Fig. 8(a) and (b) show that 30° is the optimal jet angle for lift enhancement, although the lift performance of other injection angles less than 60° is similar. As shown in Fig. 8(c) and (d), the 45° jet angle has the best aerodynamic efficiency at all studied angles of attack. Therefore, considering a lift coefficient similar to 30° and higher aerodynamic efficiency, the 45° jet angle is considered the best.

The reason why the 45° jet angle is chosen as the optimal is discussed here. Fig. 9 (a) and (b) show that the larger the jet angle, the higher the mass flow rate but the lower the jet thrust, which is different from the transition shape. This is because a large jet angle results in the component of the jet reaction force in the thrust direction decreasing and the component in the negative lift direction increasing. Fig. 10(a) and (b) show the pressure contour and streamlines of

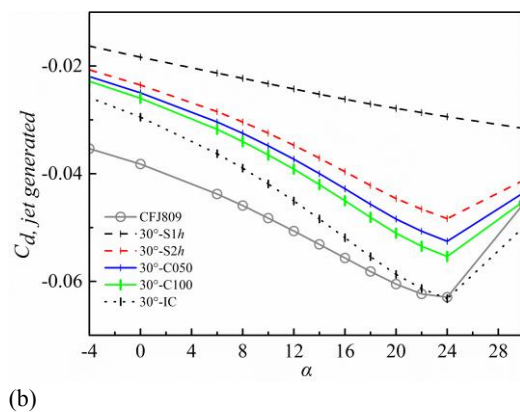


Fig. 7. Effect of transition shape: (a) mass flow rate, (b) drag coefficient generated by jet.

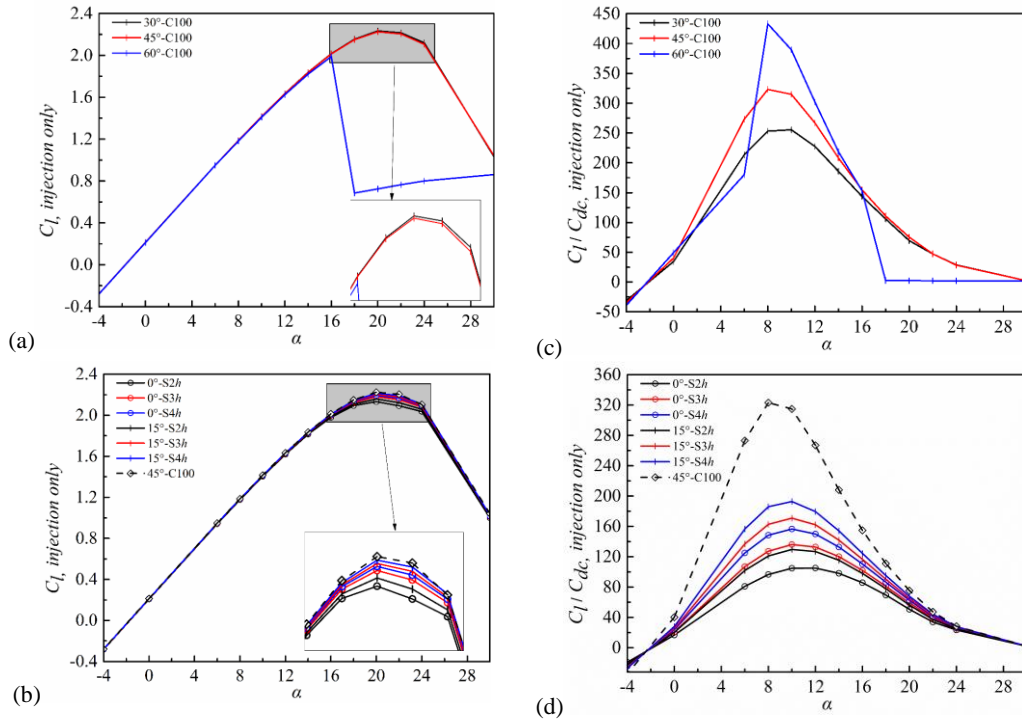


Fig. 8. Comparison of injection angles: (a) lift coefficient based on C-shape, (b) lift coefficient based on S-shape, (c) aerodynamic efficiency based on C-shape, (d) aerodynamic efficiency based on S-shape.

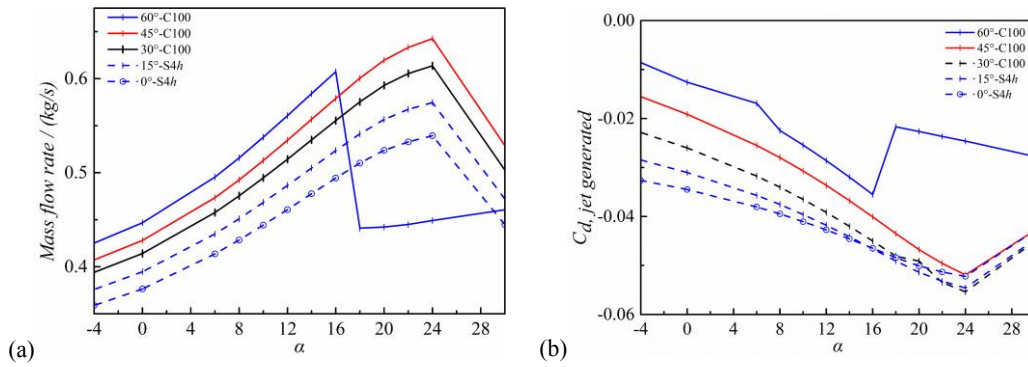


Fig. 9. Effect of jet angle: (a) mass flow rate, (b) drag coefficient generated by jet.

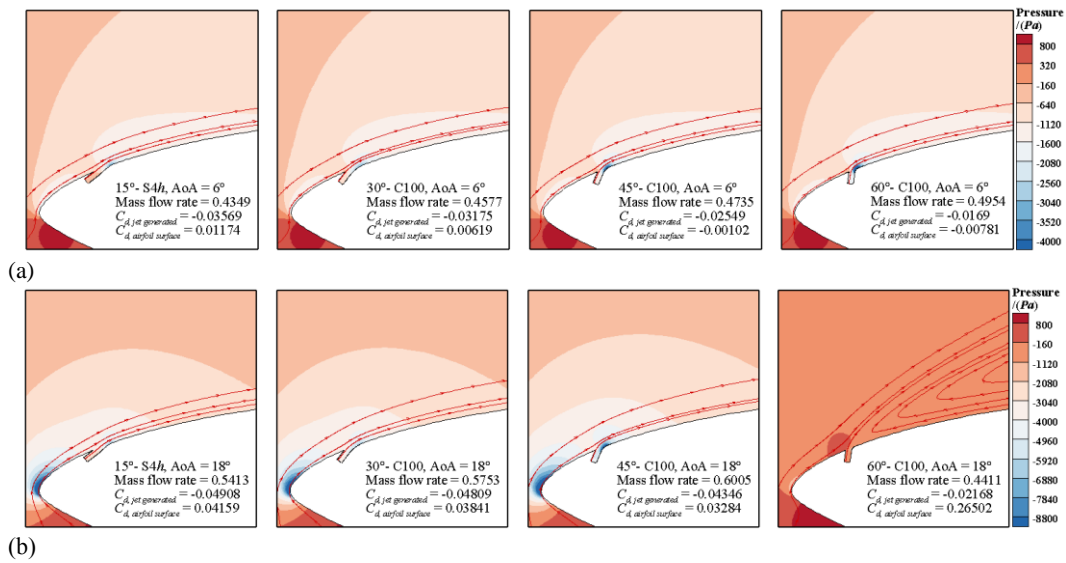


Fig. 10. Pressure contour and streamlines: (a) AoA = 6°, (b) AoA = 18°.

different jet angles when the angle of attack is 6° and 18° , respectively. When the angle of attack is 6° , the larger the jet angle, the lower the pressure at the corner from the injection slot to the upper surface. The lower pressure at the corner decreases the drag and increases the lift, which contributes to a higher lift-to-drag ratio. However, when the angle of attack is 18° , this trend is only maintained below a 45° jet angle because stall occurs when the jet angle is 60° .

In summary, when the jet angle is too large, the jet thrust and airfoil lift decrease, and it is easy to stall. When the jet angle is too small, the surface suction from the injection slot to the upper airfoil surface will decrease. To avoid stalls, a small jet angle should be used, but from the perspective of aerodynamic efficiency, there is a critical jet angle. In this paper, 45° is the critical jet angle.

4.2. Design and Analysis of Conformal Suction Slot

This section compares the parameters of the conformal suction slot based on the 45C conformal injection slot, which is the optimal conformal injection slot form defined in section 4.1. Similar to the conformal injection slot design process, the transition shapes based on the 30° suction angle were compared, and then the suction angle was investigated. As shown in Fig. 11(a) and (b), all transition shapes of the suction slot have similar lift and aerodynamic efficiency characteristics except for the two cases where the transition distance is equal to the height of the suction slot (30° -I1h and 30° -S1h). This indicates that the transition shape does not significantly affect the suction slot as long as the transition distance is sufficient. The aerodynamic efficiency comparison in Fig. 11(b) reveals that the 30° -IC shape has the highest aerodynamic efficiency, followed by the 30° -C100 shape. However, as shown in Fig. 11(c), the 30° -IC has the worst aerodynamic efficiency among all transition forms when the jet is inactive. Therefore, the C-shape (only C100 is mentioned from this point) is considered the best transition shape for the conformal suction slot.

Similar to selecting the best injection angle, the C-shape and S-shape are used to select the optimal suction angle. The results shown in Fig. 12(a) and (b) indicate that the larger the suction angle, the better the lift enhancement effect. In addition, as shown in Fig. 12(c) and (d), the aerodynamic efficiency of the 90° suction angle is the most satisfactory before and after stall, so the 90° suction angle is chosen to form a conformal slot CFJ airfoil combined with the 45C conformal injection slot.

The 90° suction angle was compared with the 30° suction angle to investigate why the 90° suction angle has the best performance. To ensure the same flow conditions in the injection slot for these two cases, the boundary conditions of the inlet of the injection duct for these two cases were set to the same total pressure (1000 Pa). As shown in Fig. 13, the lift coefficients of these two cases are similar, but the 90° suction angle has lower power consumption after the stall.

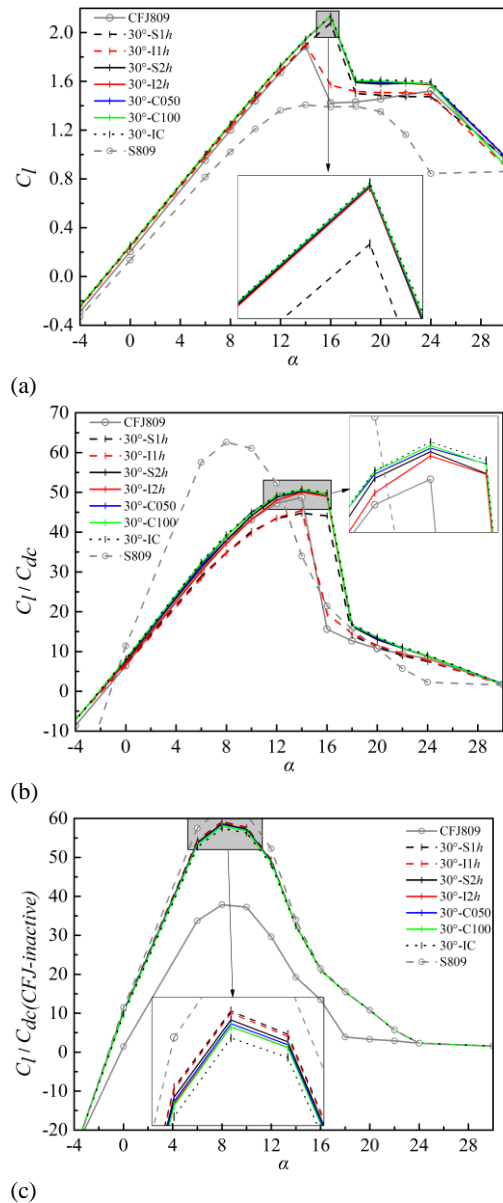


Fig. 11. Comparison of transition shapes for suction slot: (a) lift coefficient, (b) aerodynamic efficiency, (c) aerodynamic efficiency when jet is inactive.

Figure 14 shows the total pressure contours and streamlines of the 30° and 90° suction angles and reveals that the blockage zone in the suction duct of the 90° suction angle is smaller than that of the 30° case, implying that the 90° suction angle more easily absorbs the reverse flow in the separation zone. Because of the smaller blockage zone, the average total pressure in the suction slot is higher than that of the 30° suction angle. According to Eq. (6), the higher total pressure in the suction slot results in lower power consumption. In contrast, it can be speculated that the 90° suction angle requires a higher power consumption than the 30° suction angle when there is no flow separation. As demonstrated in Fig. 13, the power consumption of 90° suction is slightly higher than that of 30° suction before stall. This seems to be a drawback of the 90° suction slot and will be discussed later.

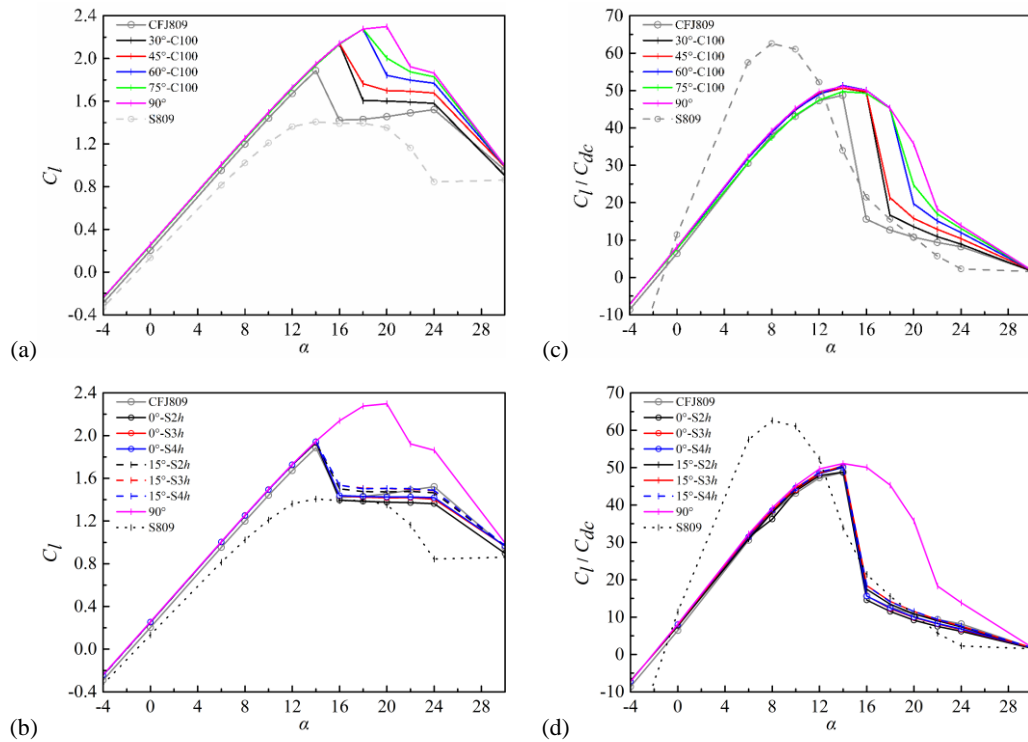


Fig. 12. Comparison of suction angles: (a) lift coefficient based on C-shape, (b) lift coefficient based on S-shape, (c) aerodynamic efficiency based on C-shape, (d) aerodynamic efficiency based on S-shape.

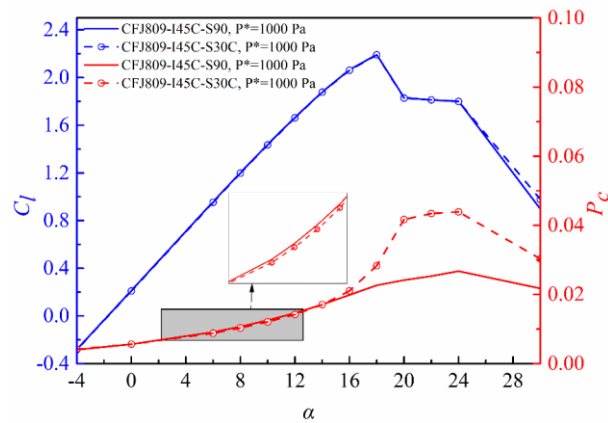


Fig. 13. Comparison between 30° and 90° suction angles under same total pressure of injection slot.

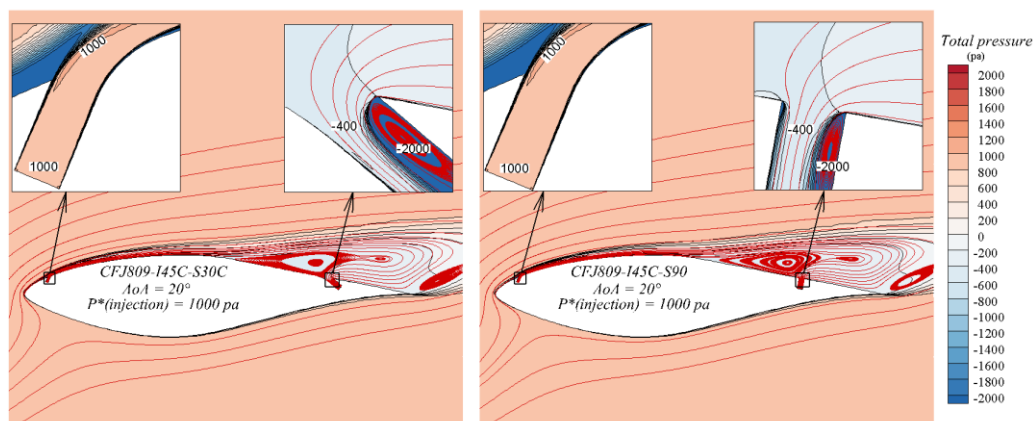


Fig. 14. Comparison of blockage area of 30° and 90° suction ducts under same total pressure of injection slot.

5. DISCUSSION

5.1. Performance of Designed Conformal Slot CFJ Airfoil with Jet Off

Figure 15 shows the aerodynamic performance of the baseline (S809), the conventional and the designed conformal slot CFJ airfoil when the jet is inactive. The lift coefficient of the conventional CFJ airfoil (CFJ809) is lower than that of the baseline and the conformal slot CFJ airfoil (CFJ809-I45C-S90). Compared with the baseline, the CFJ809-I45C-S90 airfoil has slight performance degradation in the stall region when the jet is inactive. Compared with previous studies (Chng *et al.* 2008; Zhang *et al.* 2011; Zhang *et al.* 2021b), the conformal slot CFJ airfoil designed in this paper shows a closer performance to the baseline, which benefits from the 90° suction angle that leaves the upper surface adjacent to the trailing edge unchanged. These results imply that the proposed conformal slot CFJ airfoil effectively solves the problem of the CFJ when the jet is inactive.

5.2. Performance of Designed Conformal Slot CFJ Airfoil at Different Jet Intensities

Four different momentum coefficients were studied to evaluate the flow control capability of the designed conformal slot CFJ airfoil. It can be seen in Fig. 16(a) and (b) that before the stall, the conformal slot CFJ airfoil has a higher lift coefficient than and similar aerodynamic efficiency to the conventional model. After the stall, the conformal slot CFJ airfoil always has higher aerodynamic efficiency even though the lift coefficient is already lower than the conventional CFJ airfoil when the momentum coefficients exceed 0.06. Fig. 16(c) shows that the conformal slot CFJ airfoil has higher power consumption before the stall. This is due to the more apparent blockage of the 90° suction duct, which is speculated based on Fig. 13, when no separation flow occurs on the upper airfoil surface. However, the conformal slot CFJ airfoil offers a higher lift coefficient before stall because of the same thickness and camber as the baseline, making the aerodynamic efficiency similar to that of the conventional CFJ airfoil. This means that the drawback in power consumption of the 90° suction angle before stall can be compensated by the unreduced thickness and camber. Meanwhile, the apparent lower power consumption after stall, as shown in Fig. 16(c), which benefits from the slight blockage in the 90° suction duct, makes the conformal slot CFJ airfoil maintain high aerodynamic efficiency.

Furthermore, in Fig. 16(b), an exciting phenomenon is that the conformal slot CFJ airfoil shows higher aerodynamic efficiency than the baseline before stall when the momentum coefficient is set to 0.01. In contrast, the conventional CFJ airfoil only has higher aerodynamic efficiency than the baseline after stall. This finding implies that using the conformal slot CFJ airfoil designed in this paper can not only suppress stall but also reduces the cut-in wind speed of wind turbines efficiently.

Based on the aerodynamic efficiency shown in Fig. 16(b), a control strategy using variable jet intensity is suggested. The jet momentum coefficient can be set to 0.01 when the angles of attack are lower than 8°, 0.03 when the angles of attack are between 8° and 12°, 0.06 when the angles of attack are between 12° and 16°, and 0.09 when the angles of attack are larger than 16°.

Figure 16(d) shows the pressure coefficient comparison between the baseline, conventional CFJ and conformal slot CFJ airfoil when the jet moment coefficient is 0.01 and AoA is 6°. This comparison reveals that the conventional CFJ has a higher pressure coefficient than the baseline because of the slight intensity jet between the injection and suction slot weakens the main flow. However, the conformal CFJ airfoil has the lowest pressure coefficient, benefitting from the unreduced thickness and camber and the acceleration of the jet from the slot to the upper airfoil surface. This comparison further proves that before stalling, the conformal slot CFJ has an advantage over the conventional CFJ.

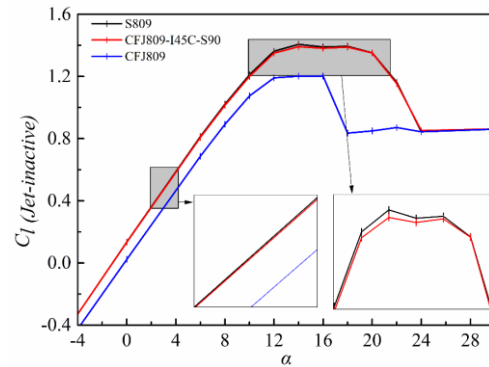


Fig. 15. Comparison between conformal slot CFJ airfoil, conventional CFJ airfoil and baseline when jet is inactive.

5.3. Effect on the Output Power of an Individual Wind Turbine

The output power coefficient of the CFJ airfoil was validated. A schematic diagram of the blade element is shown in Fig. 17(a). The output power coefficient of a blade element was calculated using the following formula:

$$P_e = \frac{\frac{1}{2} \rho_\infty W^2 c (C_l \sin \phi - C_d \cos \phi) \omega r}{\frac{1}{2} \rho_\infty W^3 c} \quad (9)$$

where $W = 51$ m/s, corresponding to the Mach and Reynolds numbers in the design process. $\omega = 7.96$ rpm when the incoming flow velocity is set to 10 m/s. r represents the blade element radius away from the centerline of the rotation plane, and the value is 60 m here. Based on the rotation speeds and the incoming flow velocity, the designed inflow angle ϕ is 11°. The angle of attack corresponding to the maximum lift-to-drag ratio of the S809 airfoil is 8°, as shown in

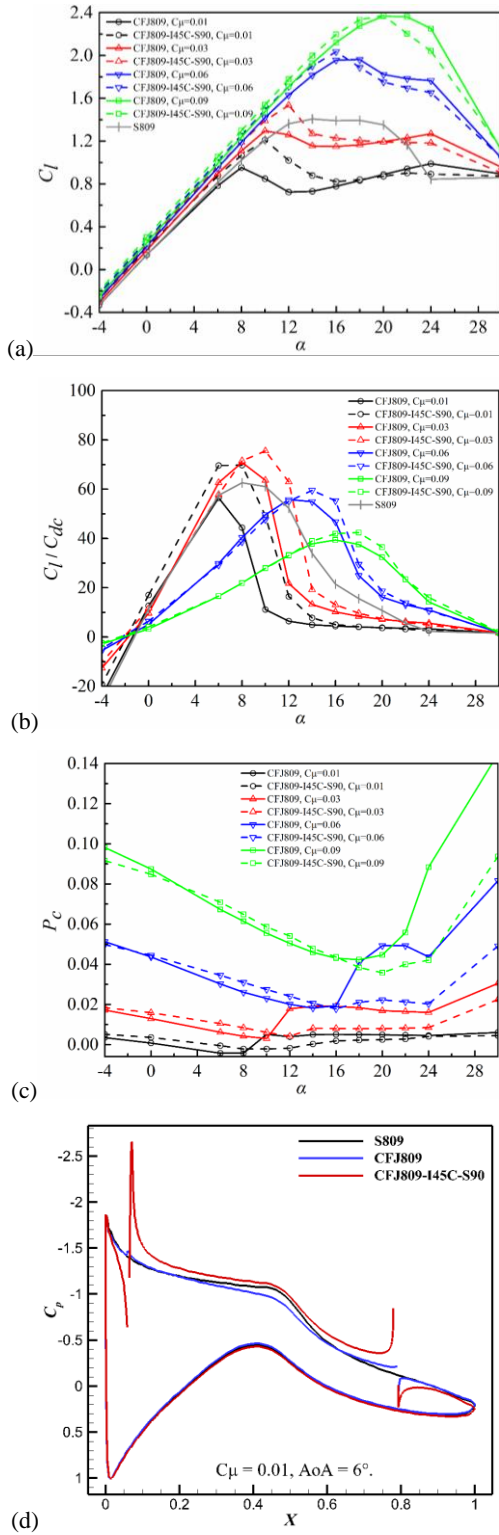


Fig. 16. Comparison between conformal slot CFJ and conventional CFJ: (a) lift coefficient, (b) aerodynamic efficiency, (c) power consumption, (d) pressure coefficient.

Fig. 16(b). Therefore, the designed pitch angle θ in Fig. 17(a) is 3° when ignoring the induced factor.

In this validation process, the resultant velocity W is constant, but the angle of attack α is changed from 0°

to 30° . The two CFJ airfoils have the same jet intensity but change with the angles of attack according to the variable jet momentum coefficient strategy of the conformal slot CFJ mentioned in Fig. 16(b) when substituting CFJ airfoils for the baseline. The blade tip speed ratio (TSR) also changes with the angles of attack, as shown in Fig. 16(b). Fig. 16(b) shows that the CFJ airfoil improved the output power after the stall of the baseline. Before the stall, the conventional CFJ airfoil (CFJ809) performs better than the baseline. However, the conformal slot CFJ airfoil designed in this paper (CFJ809-I45C-S90) has the highest output power. Compared with the baseline, the output power of the CFJ809-I45C-S90 airfoil increases by 15.86% when the angle of attack is 10° , 97.92% when the angle of attack is 20° , and 122.2% when the angle of attack is 30° . Therefore, it can be revealed that the conformal slot CFJ airfoil not only suppresses stall but also improves power generation in low-wind-speed regions. In addition, it can be inferred that for the exact output power requirements, the use of conformal slot CFJ can further reduce the blade size and alleviate the difficulty of blade structure design for large wind turbines. This will be investigated in the future.

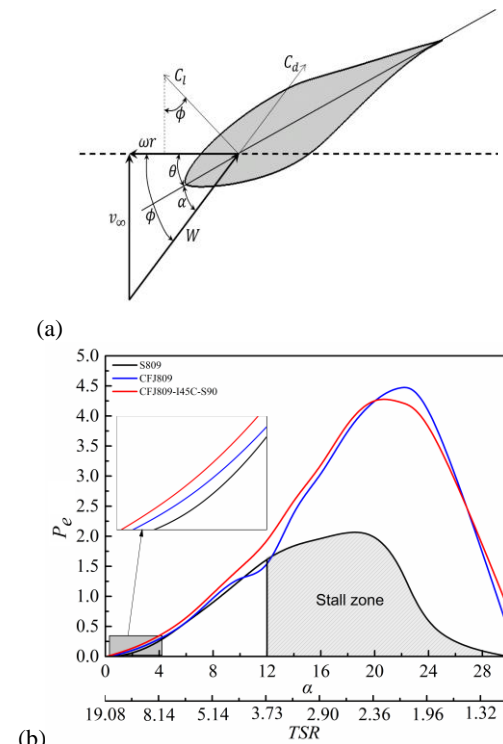


Fig. 17. Output power comparison of baseline and CFJ airfoils: (a) schematic diagram of blade element, (b) output power coefficient.

6. CONCLUSIONS

This paper proposed a general design method for the conformal slot CFJ based on slot parameters under a predetermined power consumption. The optimal parameters were investigated, and the aerodynamic performance of the designed conformal slot CFJ

airfoil under different jet intensities was checked. Finally, the output power of an individual wind turbine was evaluated when using the CFJ airfoil. The following conclusions were drawn: 1) The transition shape of the injection slot has a noticeable effect on the jet thrust and aerodynamic efficiency. The IC shape has the highest aerodynamic efficiency when the jet is active. However, the C shape was considered the best transition shape when considering the comprehensive performance of active and inactive jets. In addition, the transition distance should be greater than the slot height. 2) From the perspective of avoiding stalls, a small jet angle should be used, but from the perspective of aerodynamic efficiency, there is a critical jet angle. In this paper, 45° is the critical jet angle. 3) The transition shape of the suction slot has little effect on the CFJ airfoil. In contrast, the larger the suction angle, the higher the lift and aerodynamic efficiency. The reason is that the higher suction angle makes it easier to absorb the reverse flow if separation occurs. Moreover, the transition distance of the conformal suction slot should also be greater than the slot height. 4) The blockage of the larger suction angle before the stall can be compensated by the unreduced thickness and camber of the conformal slot design. 5) The designed conformal slot CFJ airfoil has a similar aerodynamic performance to the baseline when the jet is inactive and has a better lift coefficient and aerodynamic efficiency than the conventional CFJ airfoil when the jet is active. In addition, the designed conformal slot CFJ airfoil can offer higher aerodynamic efficiency than the baseline before stalling with a slight jet intensity. 6) Using the variable jet intensity control strategy, the conformal slot CFJ airfoil designed in this paper can suppress stall and improve power generation by more than 10% in low-wind-speed regions.

The current limitations of the CFJ lie in the motive power, installation and jet velocity. In future research, the power source is a problem to be solved. In addition, the installation of CFJ to avoid impacts of the slot on blade structures needs to be studied. Moreover, the design of the pump, which should provide an effective jet with lower power consumption, needs to be considered.

ACKNOWLEDGMENTS

This work was supported by the National Natural Science Foundation of China (Grant No. 11972306), and the 111 Project of China (B17037). The authors would also like to acknowledge the computing services from the High-Performance Computing Center of Northwestern Polytechnical University.

REFERENCES

- Aramendia, I., U. Fernández-Gámiz, J. Ramos-Hernanz, J. Sancho, J. M. López-Guede and E. Zulueta (2017). Flow Control Devices for Wind Turbines. In: Bizon, N., Mahdavi Tabatabaei, N., Blaabjerg, F., Kurt, E. (2017). Flow Control Devices for Wind Turbines. In: Bizon, N., Mahdavi Tabatabaei, N., Blaabjerg, F., Kurt, E.
- (eds) *Energy Harvesting and Energy Efficiency. Lecture Notes in Energy*, vol 37. Springer, Cham, Switzerland.
- Aubrun, S., A. Leroy and P. Devinant (2017). A review of wind turbine-oriented active flow control strategies. *Experiments in Fluids* 58(9), 1-21.
- Boling J. S. and G. C. Zha (2021, January). *Numerical investigation of longitudinal static stability of a high-speed tandem-wing VTOL vehicle using co-flow jet airfoil*. In AIAA SciTech 2021 Forum, Virtual event.
- Byrd, C. S., M. Emmanuel, D. O. Velardo, D. Stone and Wang, W. (2021, January). *Conceptual design of a high endurance rotating-wing mars exploration spacecraft (HERMES)*. In AIAA SciTech 2021 Forum, Virtual event.
- Car, D., N. J. Kuprowicz, J. Estevadeordal, Zha G. C. and W. Copenhaver (2004, June). Stator Diffusion Enhancement Using a Re-Circulating Co-Flowing Steady Jet. In *Proceeding of Asme Turbo Expo 2004*, Vienna, Austria.
- Chng, T. L., J. M. Zhang and H. M. Tsai (2008, January). A novel method of flow injection and suction for lift enhancement. In *46th AIAA Aerospace Sciences Meeting and Exhibit*, Reno, United States.
- Choudhry, A., M. Arjomandi and R. Kelso (2013). Horizontal axis wind turbine dynamic stall predictions based on wind speed and direction variability. *Proceeding of the Institution of Mechanical Engineers, Part A: Journal of Power and Energy* 227(3), 338-351.
- Dhakal, S., Y. C. Yang, G. C. Zha and J. Boiling (2017, June). Numerical investigation of low speed performance of transonic co-flow jet airfoil. In *35th AIAA Applied Aerodynamics Conference*, Denver, United States.
- Fan, Z. X. and C. C. Zhu (2019). The optimization and the application for the wind turbine power-wind speed curve. *Renewable Energy* 140(9), 52-61.
- Gad-el-Hak, M. (2000). *Flow Control: Passive, Active, and Reactive Flow Management*. Cambridge University Press, Cambs, Britain.
- Genç, M. S., U. Kaynak and H. Yapici (2011). Performance of transition model for predicting low Re aerofoil flows without/with single and simultaneous blowing and suction. *European Journal of Mechanics B-fluids* 30(3), 218-235.
- International Energy Agency (2021). World Energy Outlook 2021. Report of International Energy Agency. Paris, France.
- Johnson, S. J., J. P. Baker, V. C. P. Dam and D. Berg (2010). An overview of active load control techniques for wind turbines with an emphasis on microtabs. *Wind Energy* 13(3), 239-253.
- Johnston, J. P. and M. Nishi (1990). Vortex generator jets - Means for flow separation control. *AIAA*

- Journal* 28(6), 989-994.
- Laval, J. P., C. Braud, G. Fournier and M. Stanislas (2010). Large-eddy simulations of control of a separated flow over a 2D bump by means of pulsed jets. *Journal of Turbulence* 11(11), 1-33.
- Lefebvre, A. and G. C. Zha (2013, January). Numerical Simulation of Pitching Airfoil Performance Enhancement Using Co-Flow Jet Flow Control. In *31st AIAA Applied Aerodynamics Conference*, San Diego, United States.
- Lefebvre, A. and G. C. Zha (2014, January). Pitching Airfoil Performance Enhancement Using Co-Flow Jet Flow Control at High Mach Number. In *52nd Aerospace Sciences Meeting*, Maryland, United States.
- Liu, J., R. Chen and R. Qiu and W. Zhang (2020). Study on dynamic stall control of rotor airfoil based on coflow jet. *International Journal of Aerospace Engineering* 2020(8845924), 1-15.
- Liu, J., R. Chen and Q. Song and Z. Shi (2022a). Active flow control of helicopter rotor based on coflow jet. *International Journal of Aerospace Engineering* 2022(9299470), 1-19.
- Liu, J., R. Chen and Y. You and Z. Shi (2022b). Numerical investigation of dynamic stall suppression of rotor airfoil via improved co-flow jet. *Chinese Journal of Aeronautics* 35(3), 169-184.
- Liu, Z. X. and G. C. Zha (2016, June). Transonic airfoil performance enhancement using co-flow jet active flow control. In *8th AIAA Flow Control Conference*, Washington, D. C., United States.
- Mamouri, A. R., E. Lakzian and A. B. Khoshnevis (2019). Entropy analysis of pitching airfoil for offshore wind turbines in the dynamic stall condition. *Ocean Engineering* 187(9), 106229.1-106229.19.
- Prince, S. A., C. Badalamenti and C. Regas (2017). The application of passive air jet vortex-generators to stall suppression on wind turbine blades. *Wind Energy* 20(1), 109-123.
- Rafiuddin, N., M. Y. Saif and A. Ahmad (2018, Sept). Wind Array: A novel approach to low speed wind harnessing. In *2018 International Conference on Computing, Power and Communication Technologies (Gucon)*, Greater Noida, India.
- Shun, S. and N. A. Ahmed (2012). Wind Turbine Performance Improvements using Active Flow Control Techniques. *Procedia Engineering* 49(10), 83-91.
- Singh, R. K. and M. R. Ahmed (2013). Blade design and performance testing of a small wind turbine rotor for low wind speed applications. *Renewable Energy* 50(8), 812-819.
- Somers, D. M. (1997). *Design and experimental results for the S809 airfoil*. NREL/SR-440-6918, the National Renewable Energy Laboratory. Fort Collins, United States.
- Van Dam, C. P., D. E. Berg and S. J. Johnson (2008). Active Load Control Techniques for Wind Turbines. SAND2008-4809, the Sandia National Laboratories, Albuquerque, United States.
- Wang, Y. and G. C. Zha (2019, June). Study of super-lift coefficient of co-flow jet airfoil and its power consumption. In *AIAA Aviation 2019 Forum*, Dallas, United States.
- Wu, T., B. F. Song, W. P. Song, W. Q. Yang and Z. H. Han (2020). Aerodynamic performance enhancement for flapping airfoils by co-flow jet. *Chinese Journal of Aeronautics* 33(10), 2535-2554.
- Xu, H. Y., C. L. Qiao and Z. Y. Ye (2016). Dynamic Stall Control on the Wind Turbine Airfoil via a Co-Flow Jet. *Energies* 9(6), 429.1-429.25.
- Xu, H. Y., S. L. Xing and Z. Y. Ye (2015). Numerical study of the S809 airfoil aerodynamic performance using a co-flow jet active control concept. *Journal of Renewable and Sustainable Energy* 7(2), 023131.1- 023131. 21.
- Xu, K. W. and G. C. Zha (2020, June). Investigation of Coflow Jet Active Flow Control for Wind Turbine. In *AIAA Aviation 2020 FORUM*, Virtual Event.
- Xu, K. W. and G. C. Zha (2021, June). High efficiency wind turbine using co-flow jet active flow control. In *Proceedings of ASME Turbo Expo 2021*, Virtual event.
- Xu, K. W., J. H. Zhang and G. C. Zha (2019, January). Drag minimization of co-flow jet control surfaces at cruise conditions. In *AIAA Scitech 2019 Forum*, San Diego, United States.
- Yang, Y. C. and G. C. Zha (2017, January). Super-lift coefficient of active flow control airfoil: what is the limit?. In *55th AIAA Aerospace Sciences Meeting*, Grapevine, United States.
- Yang, Y. C. and G. C. Zha (2018, January). Numerical investigation of ultra-high lift coefficient co-flow jet flow control wing. In *2018 AIAA Aerospace Sciences Meeting*, Kissimmee, United States.
- Yang, Y. C. and G. C. Zha (2018, June). Numerical investigation of performance improvement of the co-flow jet electric airplane. In *2018 Applied Aerodynamics Conference*, Atlanta, United States.
- Yang, Y. C. and G. C. Zha (2019, January). Conceptual design of the co-flow jet hybrid electric regional airplane. In *AIAA SciTech 2019 Forum*, San Diego, United States.
- Zha, G. C. and B. F. Carroll, C. D. Paxton, C. Conley and A. P. Wells (2007). High-Performance Airfoil Using Coflow Jet Flow Control. *AIAA Journal* 45(8), 2087-2090.

- Zha, G. C., C. D. Paxton and C. Gables (2004, July). A Novel Airfoil Circulation Augment Flow Control Method Using Co-Flow Jet. In *2nd AIAA Flow Control Conference*, Portland, United States.
- Zha, G. C., C. D. Paxton, A. P. Wells and B. F. Carroll (2006). Effect of Injection Slot Size on the Performance of Coflow Jet Airfoil. *Journal of Aircraft* 43(4), 987-995.
- Zhang, J. M., T. L. Chng and H. M. Tsai (2011). Performance of Coflow Jet Airfoils with Conformal Slot Geometries. *Journal of Aircraft* 48(3), 1107-1112.
- Zhang, X. L., X. D. Yang and B. F. Song (2021a). Numerical investigation of performance enhancement of the S809 airfoil and phase VI wind turbine blade using co-flow jet technology. *Energies* 14(10), 6933.1-6933.20.
- Zhang, Y. Z., H. Y. Xu, Y. W. Chu and Y. Xu (2021b). Two-Dimensional Numerical Study of the Pulsed Co-Flow Jet. *Fluid Dynamics* 56(6):361-370.
- Zhi, H. L., Z. H. Zhu, Y. L. Lu, S. Deng and T. Xiao (2021). Aerodynamic performance enhancement of co-flow jet airfoil with simple high-lift device. *Chinese Journal of Aeronautics* 34(9), 143-155.
- Zhu, C. Y., Y. N. Qiu and T. G. Wang (2021). Dynamic stall of the wind turbine airfoil and blade undergoing pitch oscillations: A comparative study. *Energy* 222(5), 120004.1-120004.14.